

Doppler Profiler and Radar Observations of Boundary Layer Variability during the Landfall of Tropical Storm Gabrielle

KEVIN R. KNUPP AND JUSTIN WALTERS

Department of Atmospheric Science, University of Alabama in Huntsville, Huntsville, Alabama

MICHAEL BIGGERSTAFF

School of Meteorology, University of Oklahoma, Norman, Oklahoma

(Manuscript received 20 January 2004, in final form 14 February 2005)

ABSTRACT

Detailed observations of boundary layer structure were acquired on 14 September 2001, prior to and during the landfall of Tropical Storm Gabrielle. The Mobile Integrated Profiling System (MIPS) and the Shared Mobile Atmospheric Research and Teaching Radar (SMART-R) were collocated at the western Florida coastline near Venice, very close to the wind center at landfall. Prior to landfall, the boundary layer was rendered weakly stable by a long period of evaporational cooling and mesoscale downdrafts within extensive stratiform precipitation that started 18 h before landfall. The cool air mass was expansive, with an area within the 23°C surface isotherm of about 50 000 km². East-northeasterly surface flow transported this cool air off the west coast of Florida, toward the convergent warm core of the Gabrielle, and promoted the development of shallow warm and cold fronts that were prominent during the landfall phase.

Airflow properties of the boundary layer around the coastal zone are examined using the MIPS and SMART-R data. Wind profiles exhibited considerable temporal variability throughout the period of observations. The stable offshore flow within stratiform precipitation exhibited a modest jet that descended from about 600 to 300 m within the 20-km zone centered on the coastline. In contrast, the onshore flow on the western side of the wind center produced a more turbulent boundary layer that exhibited a well-defined top varying between 400 and 1000 m MSL. The horizontal variability of each boundary layer is examined using high-resolution Doppler radar scans at locations up to 15 km on either side of the coastline, along the mean flow direction of the boundary layer. These analyses reveal that transitions in boundary layer structure for both the stable and unstable regimes were most substantial within 5 km of the coastline.

1. Introduction

Comprehensive measurements of atmospheric boundary layer (ABL) properties within tropical cyclones (TCs) have been sparse over both the ocean and coastal regions. On occasion, research aircraft have flown below 500 m MSL in special experiments to examine ABL properties and the effects of rainbands and convective cells on ABL airflow and thermodynamic fields (Moss and Merceret 1976; Barnes et al. 1983; Powell 1990a,b; Barnes and Powell 1995). ABL wind profiles and their horizontal variability have received

attention over recent years because of their importance in operational wind estimation (Powell and Black 1990; Powell et al. 1996; Dunion et al. 2003; Franklin et al. 2003) and the clues they provide on low-level dynamical processes (Kepert 2001; Kepert and Wang 2001). Over oceanic regions, GPS dropsondes have revealed high resolution vertical profiles with significant vertical structure and the presence of wind maxima below altitudes of several hundred meters (Franklin et al. 2003).

During landfall, additional asymmetries are introduced in the ABL by discontinuities in surface properties, such as increased roughness and decreased heat and moisture fluxes over land. The increase in roughness reduces surface winds (Moss and Merceret 1976; Powell 1982, 1987; Powell et al. 1991; Powell and Houston 1998), and leads to development of an internal boundary layer for both onshore and offshore flow re-

Corresponding author address: Kevin Knupp, Dept. of Atmospheric Science, University of Alabama in Huntsville, Huntsville, AL 35899.
E-mail: kevin@nsssc.uah.edu

gimes. This land–water asymmetry also changes the force balance within the ABL and produces spatial variability in ABL wind profiles (Kepert 2001; Kepert and Wang 2001; Chen and Yau 2003). While numerical simulations of landfalling hurricanes can provide a wealth of information on ABL processes and effects (Jones 1987; Tuleya 1994; Li et al. 1997; Zhang et al. 1999; Wu 2001; Chen and Yau 2003), validation of numerical models, and future improvements of model subgrid-scale parameterizations for the high-wind hurricane environment (Braun and Tao 2000), requires detailed observations (Marks et al. 1998).

Most prior investigations of the landfalling hurricane ABL have been limited to analyses of surface properties. More recently, operational fixed-base instrumentation, such as the Weather Surveillance Radar-1988 Doppler (WSR-88D) radar, has been used to determine wind profiles within and above the ABL during hurricane landfall (e.g., Marks 2003) and to examine other hurricane properties (Dodge et al. 1999; Blackwell 2000). The use of surface-based mobile instrumentation has been emphasized by Marks et al. (1998) to advance understanding of ABL properties. Specialized mobile instruments, including 10-m towers, mobile Doppler radars, and the Mobile Integrated Profiling System (MIPS), have been used in recent years to acquire targeted measurements of landfalling hurricanes. For example, recent measurements by mobile Doppler radars within high winds of landfalling TCs have revealed finescale lineal features in radial velocity measurements over the lowest several hundred meters that appear similar to ABL rolls (e.g., Wurman and Winslow 1998). Details on ABL properties observed by a 915-MHz Doppler wind profiler during the landfall of Hurricane Georges (1998) are summarized in Knupp et al. (2000). Using airborne Doppler data, Geerts et al. (2000) also documented the landfall of Hurricane Georges over the Dominican Republic, which involved explosive growth of deep convection and release of copious rainfall over mountainous regions.

To date, however, a detailed understanding of 3D ABL changes during landfall remains incomplete. Improved knowledge of the ABL processes have important connections to (i) hurricane intensity change; (ii) improved knowledge of the ABL over water, land, and the differences between the two; (iii) improved parameterizations in numerical models; and (iv) improvements in quantitative precipitation forecasting and even quantitative precipitation estimation.

On 14 September 2001, Tropical Storm (TS) Gabrielle underwent rapid transformation during landfall on the western Florida coast near Venice. Special observing platforms [associated with Fourth Convection and

Moisture Experiment (CAMEX-4)], including the University of Alabama in Huntsville (UAH) MIPS and the Shared Mobile Atmosphere Research and Teaching Radar (SMART-R), acquired high-resolution datasets that documented ABL and mesoscale airflow very near the point of landfall. The observations presented in this paper examine the spatial/temporal variability in ABL structure that occurred around the time of landfall.

Section 2 describes the instrumentation used in the study. Section 3 provides an overview of the mesoscale characteristics of TS Gabrielle around the time of landfall in order to place the observed surface and ABL properties in proper context. Section 4 considers surface properties during landfall and addresses two questions. (i) What is the impact of cold air production over land on intensity change during landfall? (ii) What is the role of boundaries during the landfall process, and under what conditions are boundaries produced? Section 5 examines ABL spatial/temporal variability with Doppler radar and profiler observations, and focuses on two additional questions. (iii) What are the ABL temporal variability properties at a fixed point at the coastline? (iv) How do the ABL properties change from offshore to onshore flow regimes?

2. Data sources

One of the goals of CAMEX-4 was to improve understanding of processes and impacts associated with landfalling tropical storms and cyclones. Ground-based mobile facilities were assembled to supplement measurements from aircraft. These included the SMART-R (a mobile C-band Doppler radar), the X-band polarimetric radar on wheels (X-POW; University of Connecticut), and the MIPS. Measurements from the X-POW did not materialize for this mission because of technical problems. Likewise, aircraft operations were not conducted because landfall occurred much sooner than forecast.

The SMART-R and MIPS setup near the Venice airport on 14 September 2001 at 0235 and 0400 UTC, respectively, at locations about 1 km apart. The MIPS site was located about 100 m from the coastline. The primary MIPS dataset used in this paper is derived from the 915-MHz wind profiler, which sampled to about 11 km AGL. The vertical beam was sampled every 60 s, and the dwell time for all beams was about 30 s. The SMART-R scanned primarily full-volume (360°) scans continuously at elevations defined in Table 1. Obstructions from trees and the radar truck cab were somewhat problematic at low elevation angles, particularly in the eastern semicircle (the land side). Reflectivity factor

TABLE 1. Elevation angles used by the SMART-R, which scanned full 360° circles.

Time period	Scan type	No. of elevations	Scan time (min)	No. of elevations	Elevation angles (deg)
0545–0918 UTC	Volume (360°)	17	5.7	17	0.8, 1.7, 2.9, 4.4, 6.0, 7.7, 9.5, 11.5, 13.7, 16.1, 18.7, 21.7, 25.2, 29.2, 33.7, 38.7, 44.2
0924–1317 UTC	Volume (360°)	11	4.2	11	0.8, 1.7, 2.9, 4.4, 6.0, 7.7, 9.5, 11.5, 13.7, 16.1, 18.7
1322–1500 UTC	Volume (360°)	13	5.0	13	0.8, 1.7, 2.9, 4.4, 6.0, 7.7, 9.5, 11.5, 13.7, 16.1, 18.7, 21.7, 25.2

(Z) and radial velocity (V_r) data were collected at range gate intervals of 133 m and azimuth intervals of about 1°. The radar beamwidth is about 1.5°. The SMART-R was located 70 km south of the Tampa Bay WSR-88D radar, which was scanning in the Volume Coverage Pattern Eleven (VCP-11) scan mode.

Surface data from 32 National Weather Service (NWS) Automated Surface Observing Systems (ASOS) and four Florida Agricultural Weather Network (FAWN) sites were analyzed to determine surface properties over the Florida Peninsula. Most of the ASOS data had a default 1-h sampling frequency for all standard meteorological variables and cloud base, but additional supplemental observations within the 1-h period were relatively frequent. FAWN data have a uniform 15-min temporal sampling period of standard meteorological variables, solar radiation, and soil temperature. Several supplementary buoy (National Data Buoy Center and University of South Florida) and Coastal-Marine Automated Network (C-MAN) sites were used to determine offshore and coastal conditions at locations near the point of landfall.

3. Mesoscale evolution and precipitation properties

a. Precipitation distribution and mesoscale flows

Gabrielle exhibited a period of rapid intensification, followed by rapid weakening, during the 12-h period (0000–1200 UTC) before landfall. Although Gabrielle was classified as a strong TS, both aircraft reconnaissance and Doppler radar measurements suggest that Gabrielle may have intensified to a marginal category 1 hurricane by 1000–1100 UTC (1–2 h prior to landfall) on 14 September 2001. Molinari et al. (2006) provide details on this rapid intensification. A rapid weakening occurred after 1100 UTC because of a combination of effects, some of which are considered in section 4. Thus, Gabrielle was a distinctly unsteady tropical storm during the period of observations.

The general pattern of intensity change—strengthening followed by weakening—between 0000 and 1200 UTC is portrayed in Geostationary Operational Envi-

ronmental Satellite (GOES)-enhanced infrared (IR) imagery presented in Fig. 1. Even 12 h prior to landfall, at 0015 UTC, Gabrielle was a rather disorganized convective system (Fig. 1a). By 0645 UTC, rapid intensification was indicated by cold cloud-top temperatures closer to the wind center¹ (Figs. 1b,c); active cloud-to-ground (CG) lightning activity that appeared within vigorous deep convection immediately downshear of the wind center (Molinari et al. 2006); and a general increase in cyclonic circulation, measured by reconnaissance aircraft between 0600 and 0900 UTC (Molinari et al. 2006), and by the WSR-88D and SMART-R Doppler radars between 0900 and 1100 UTC.

During the 0645–1200 UTC period, Gabrielle exhibited improved organization, but prominent asymmetry was still apparent; for example, the wind center was located on the upshear (southwest) flank of the centroid of cold cloud-top temperatures (Figs. 1b,c). A broad area of cold cloud tops is also shown extending to the northeast (downshear) from Gabrielle's core. A rapid weakening of deep convection occurred during the 1100–1815 UTC period, and by 1815 UTC, deep convection around the wind center had disappeared (Fig. 1d). At this time, much of the central Florida Peninsula was void of clouds with brightness temperatures less than 270 K, although extensive precipitating stratiform clouds at slightly warmer temperatures did exist over this region. In the next section, this rapid demise is related to the presence of very cool air that had developed prior to landfall over this part of the Florida Peninsula.

The evolution of precipitation around the landfall point is depicted by equivalent reflectivity factor (Z) images presented in Fig. 2. The rapid intensification stage was accompanied by vigorous deep convection (regions with Z exceeding 45 dBZ at 0601 and 0801 UTC) downshear of the wind center. A broad strati-

¹ The wind center, estimated from animations of WSR-88D reflectivity and Doppler velocity data, is defined as the apparent center of the wind circulation relative to the ground (Harasti et al. 2004).

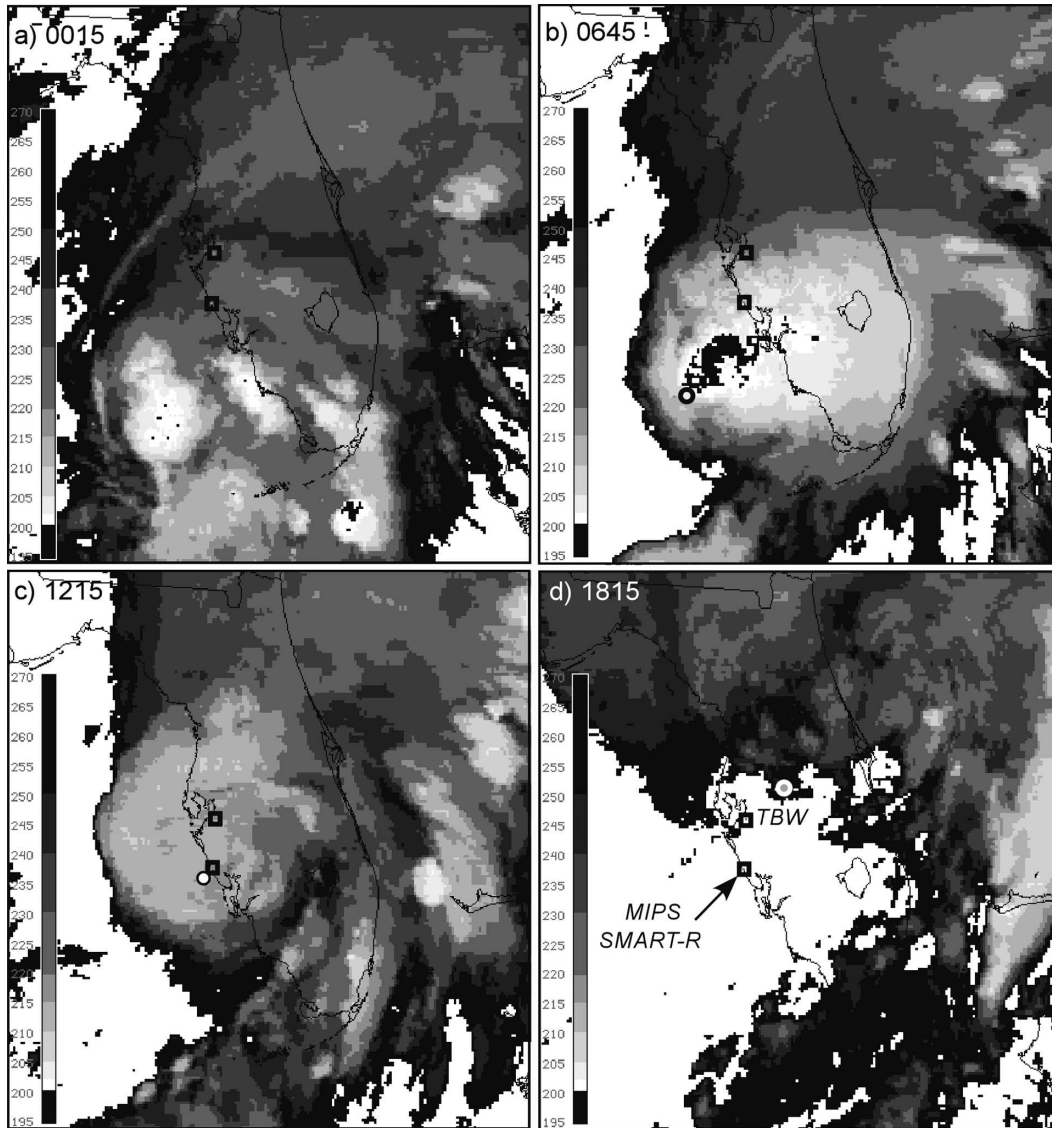


FIG. 1. GOES-enhanced IR imagery at (a) 0015, (b) 0645, (c) 1215, and (d) 1815 UTC 14 Sep 2001. (b)–(d) The approximate location of the wind center is denoted by a filled circle. The grayscale on the left defines brightness temperature (K). Instrument locations are identified in (d). The distance between the TBW WSR-88D and SMART-R radars is 70 km.

form region appears as a separate entity north and northeast of the convective region during the 0600–1000 UTC interval, and stratiform precipitation extended over much of central and northern Florida during this period. During the latter part of this sequence, beginning near 1200 UTC, a dry intrusion wrapped around the southern and eastern side of the circulation (Figs. 2d,e).

Soundings from Tampa Bay (TBW) at 0600, 1200, and 1800 UTC (Fig. 3) reveal a temperature profile that was weakly stable to neutral with respect to saturated air, with the following exceptions. The 0600 UTC

sounding sampled stratiform precipitation 210 km north-northeast of the wind center. This sounding shows a slightly subsaturated layer below 80 kPa, which would have supported evaporation within inferred mesoscale downdrafts. An elevated moist absolutely unstable layer (MAUL; Bryan and Fritsch 2000) is centered near the top of this layer near 80 kPa. The 1200 UTC sounding (70 km north of the wind center) is completely saturated throughout its depth. Another MAUL is centered near 58 kPa and caps a region of significant warming that had occurred over the previous 6 h. Warming of this layer is consistent with a veering wind

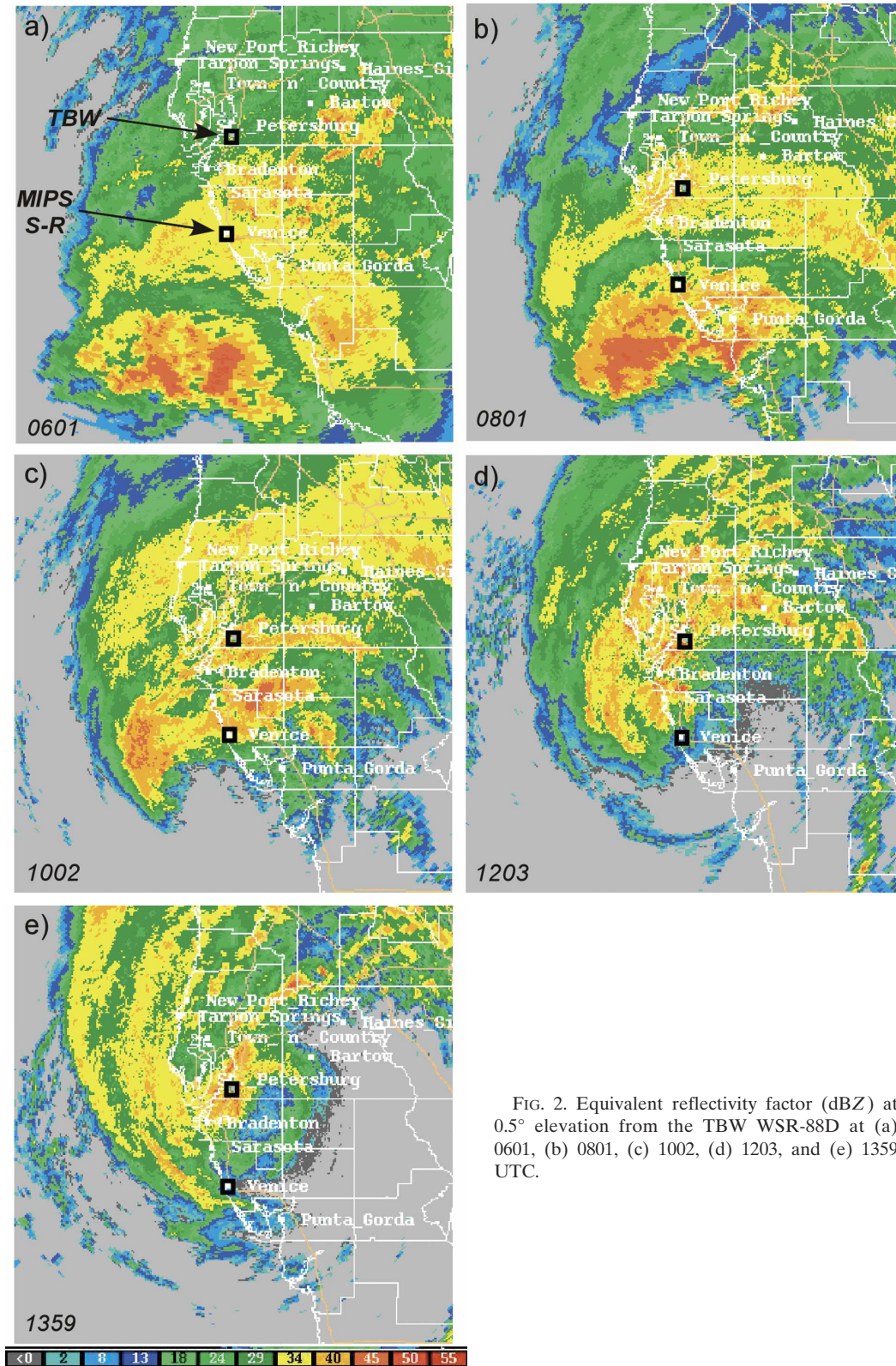


FIG. 2. Equivalent reflectivity factor (dBZ) at 0.5° elevation from the TBW WSR-88D at (a) 0601, (b) 0801, (c) 1002, (d) 1203, and (e) 1359 UTC.

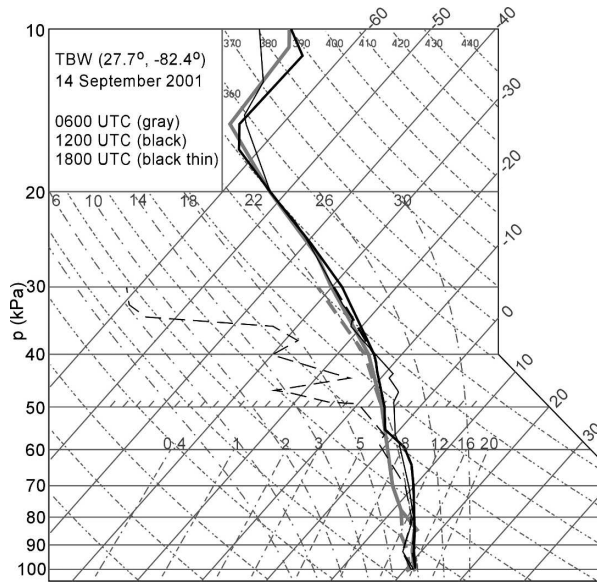


FIG. 3. Soundings from TBW at 0600, 1200, and 1800 UTC, plotted on a skew T -log p diagram. The TBW location is shown in Figs. 1 and 2.

profile,² suggesting warm advection within the stratiform precipitation region.

The 1800 UTC TBW sounding (60 km southwest of the wind center) reveals considerable drying above the cloud top near 65 kPa (near 0°C). Entrainment of dry air into the circulation at upper levels also likely played a role in the rapid weakening of Gabrielle around and after landfall. Most vigorous flow was confined to levels below 70 kPa. This sounding reveals an ABL about 500 m deep, capped by an absolutely stable layer between 92 and 80 kPa.

b. MIPS observations during landfall

The wind center of Gabrielle passed very close to the MIPS and SMART-R. A time versus height section of 915-MHz profiler spectral moments is presented in Fig. 4 for the 12-h period 0400–1600 UTC. This figure is annotated with the following regimes, using objective criteria developed by Williams et al. (1995):

- (i) the mature stage of the leading stratiform precipitation (0500–0700 UTC);
- (ii) a period of convective and mixed convective/

² The 1200 UTC sounding reveals veering between 900 and 300 hPa, which implies warm advection assuming that the winds are in geostrophic balance. The winds were not in geostrophic balance, since the centrifugal acceleration is about 50% the magnitude of the pressure gradient force [i.e., the Rossby number, $Ro = V/(f_0R)$, is in the range 3–4].

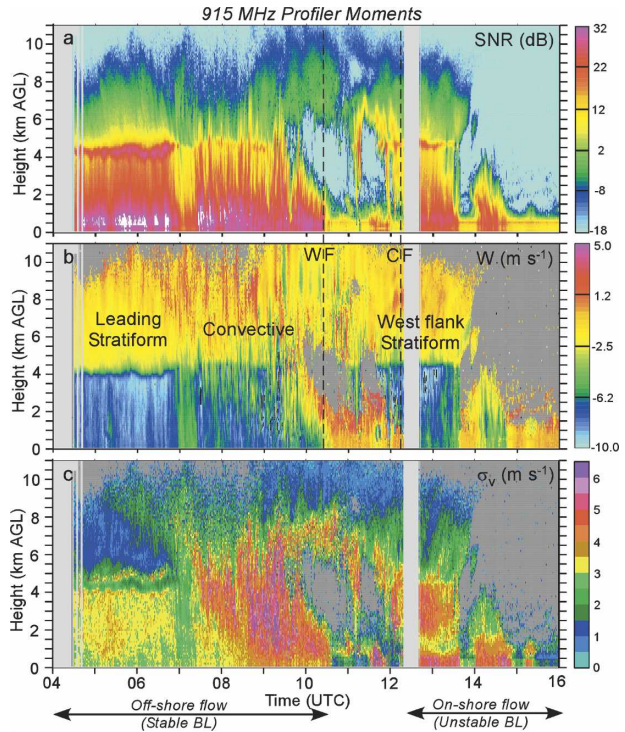


FIG. 4. Time vs height sections of 915 Doppler wind profiler parameters at vertical incidence: (a) signal-to-noise ratio (SNR, dB), (b) total vertical motion, $W = w + V_T$ ($m s^{-1}$), and (c) spectrum width ($m s^{-1}$).

stratiform precipitation, represented by greater variability in W (Fig. 4b) and enhanced spectrum width within the 1–8 km AGL layer (Fig. 4c), between 0700 and 1130 UTC;

- (iii) a period of no precipitation during the passage of the wind center over the MIPS (1030–1230 UTC);
- (iv) west flank stratiform precipitation, followed by shallow rainbands during 1230–1500 UTC.

Wind profiles for the 0500–1200 UTC period (Fig. 5) show a low-level, easterly flow that veered with height, consistent with the warming indicated in the 0600–1200 UTC TBW soundings. Likewise, the northwesterly flow measured after the wind center passed (1300 UTC) backed with height, consistent with cold advection. Relatively strong flow exceeding $25 m s^{-1}$ over the lowest 2 km was sampled within 3 h of landfall at 1200 UTC. The easterly flow was associated with cool, off-shore flow; the northwesterly flow after 1200 UTC supported a warmer onshore flow and more unstable ABL conditions. The onshore, turbulent ABL appears to be well marked by enhanced spectral width below about 600 m AGL after 1230 UTC (Fig. 4c). A similar signature was not apparent during the more stable (less turbulent) offshore flow regime prior to 1200 UTC.

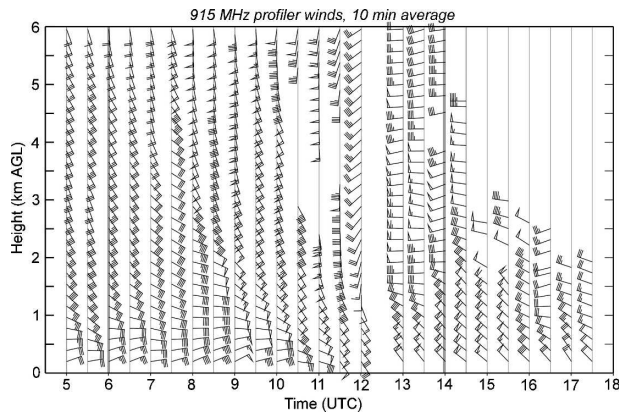


FIG. 5. Wind profiles derived from the 915-MHz profiler based on 10-min averages plotted every 30 min. A full wind barb represents 5 m s^{-1} , and a flag represents 25 m s^{-1} . The wind center passed over the MIPS site at about 1215 UTC.

4. Surface cooling and its impact on the ABL

In this section, the surface properties over the Florida Peninsula during the landfall of Gabrielle are examined. The temporal and spatial ABL properties are analyzed in section 5. Surface analyses presented in Figs. 6–8 document two significant features that affected ABL processes during the landfall period.

- (i) An extensive area of very cool air was generated by prolonged cloudiness and evaporation of stratiform rain prior to landfall. The large area of cool air exerted impacts on ABL processes and storm intensity changes around landfall time.
- (ii) As Gabrielle made landfall, boundaries resembling warm and cold fronts were produced. The generation of these boundaries was dependent on the presence of cool surface air.

a. Cool surface air

A prolonged production of cool surface air was promoted by overcast conditions and evaporation of stratiform precipitation that began about 18 h before landfall. Much of the Florida Peninsula experienced overcast conditions on 13 September, and light stratiform rain formed over this region by 1800 UTC 13 September. The surface analyses in Figs. 6a–c reveal that light to heavy rainfall, and very cool surface temperatures were particularly common over the northern two-thirds of the Florida Peninsula at 0553, 0853, and 1153 UTC. Land temperatures of 21° – 22°C are unusually cold for Gulf Coast and Florida landfalling tropical cyclones, particularly for a limited land area such as the Florida Peninsula. Cooling over the adjacent water was much less (e.g., buoy 41009 off the east Florida coast) because

of compensating surface heat fluxes over water. This air mass is colder and more extensive than that documented in other cases. Some notable examples include Hurricanes Frederic (1979) and Alicia (1983), each which developed a limited area, about 5000 km^2 or less, of cool air ($<23^{\circ}\text{C}$) on the left flank around landfall time (Powell 1982, 1987). In contrast, the area within the 23°C isotherm for Gabrielle ($\sim 50\,000 \text{ km}^2$) was about one order of magnitude larger.

The ABL over Florida and adjacent coastal waters was stabilized by prolonged evaporational cooling within (inferred) mesoscale downdrafts of the leading stratiform region. The presence of downdrafts is supported by a decreasing trend in surface θ_e over this region, and is further corroborated by a general increase in easterly flow (Figs. 6a,b) from Melbourne (MLB) on the east coast, westward through Ona and Sarasota (SRQ) on the west coast. Such flow implies mesoscale divergence in the east to northeasterly surface winds across the central Florida Peninsula.

Figure 7 presents a time series of parameters related to the ABL energetics, including solar radiation, 15-min rainfall, temperature, and equivalent potential temperature (θ_e) at Ona, located about 50 km northeast of the MIPS (see Fig. 6). Total solar radiation remained below 200 W m^{-2} during the solar cycle on 13 September (Fig. 7a), and stratiform rain started by 1600 UTC. As the stratiform rain and embedded showers intensified, θ_e decreased from 350–353 to 342–345 K near 0000 UTC, and remained within this range as stratiform rain, followed by more intense convective rain, continued until about 1200 UTC. Thus, widespread development of cool air prior to landfall was facilitated by insignificant solar radiation and by evaporational cooling within mesoscale downdrafts under the canopy of extensive stratiform precipitation downshear from Gabrielle's core.

b. Boundaries

We hypothesize that the generation of cool surface air produced horizontal temperature contrasts within the coastal zone, that later transformed to boundaries (fronts) in the ABL around landfall time. At 1115 UTC, a “warm” front increased θ_e from about 343 to 352 K at Ona (Fig. 7). This was followed by a “cold” frontal passage 2 h later, and advection of cool, drier air that reduced θ_e to values below 340 K for the remainder of 14 September. Because distinct fronts associated with low-latitude landfalling tropical storms and hurricanes have not been documented in previous studies, and represent significant ABL heterogeneity, the formation and evolution of these features is examined in greater detail in the following subsections.

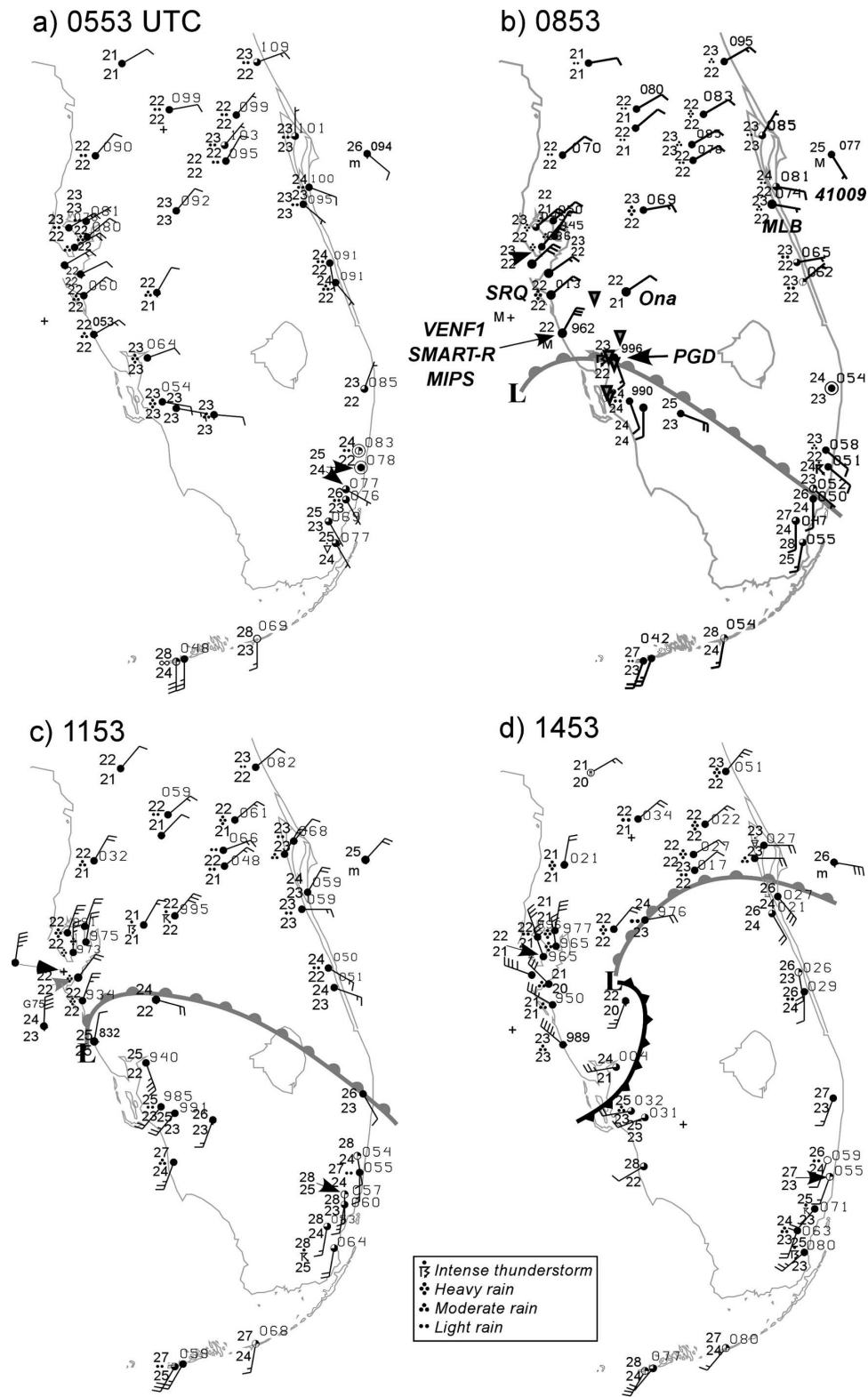


FIG. 6. Surface analyses at (a) 0553, (b) 0853, (c) 1153, and (d) 1453 UTC 14 Sep 2001. Temperature and dewpoint are plotted in $^{\circ}\text{C}$; full wind barbs represent 5 m s^{-1} . Pressure is coded in the upper right, in units of hPa according to standard convention (e.g., 082 = 1008.2 hPa, 940 = 994.0 hPa). Warm and cold frontal symbols represent boundaries that behave like warm and cold fronts. (b) Surface sites referred to in the text are identified. The MIPS and SMART-R locations are coincident with the Venice C-MAN station (VENF1).

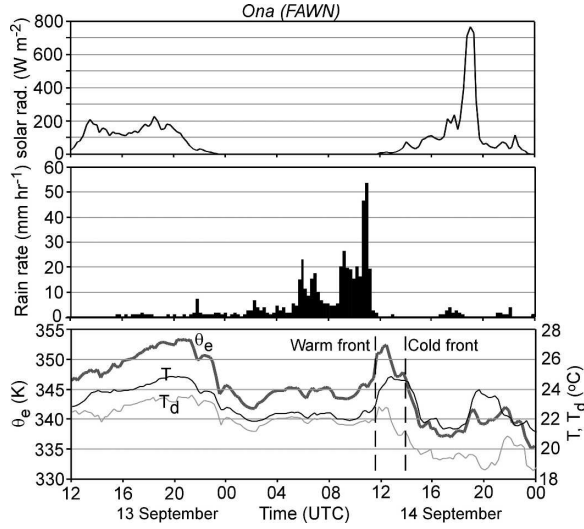


FIG. 7. Time series selected quantities from Ona, whose location is shown in Fig. 6b: (a) solar radiation, (b) rainfall rate, and (c) temperature, dewpoint, and equivalent potential temperature for the 36-h period 1200 UTC 13 Sep to 0000 UTC 15 Sep 2001. Temporal resolution is 15 min.

1) FRONTOGENESIS

For a 12-h period prior to landfall, northeasterly flow transported cool air (22°C) over warm coastal water (28°C) toward Gabrielle (Fig. 6). Surface conditions and frontal behavior from the C-MAN station at Venice, located very close to the MIPS, are displayed in Fig. 8. Following Cione et al. (2000) a standard bulk aerodynamic expression was used to estimate the heat flux (over the coastal waters),

$$H_s = \rho c_p c_h (T_{\text{water}} - T) V_{10}, \quad (1)$$

where ρ is air density, c_p is the specific heat of air at constant pressure, T_{water} is the water temperature, T is the air temperature at 10 m, V_{10} is the horizontal wind speed at 10 m, and c_h is the dimensionless coefficient of heat exchange at 10 m. Cione et al. (2000) used an expression for c_h that applies for strong wind,

$$c_h = (a + bV_{10}) \times 10^{-3},$$

where a and b are empirically determined constants with values $a = 0.75$ and $b = 0.067$. Hourly values of H_s are plotted in Fig. 8.

A surface heat flux represents a diabatic heating source ($H_s = dQ/dt$) that drives a corresponding enthalpy change rate $c_p(dT/dt)$ according to the first law of thermodynamics, expressed as

$$\frac{dQ}{dt} = c_p \frac{dT}{dt} - \alpha \frac{dp}{dt}, \quad (2)$$

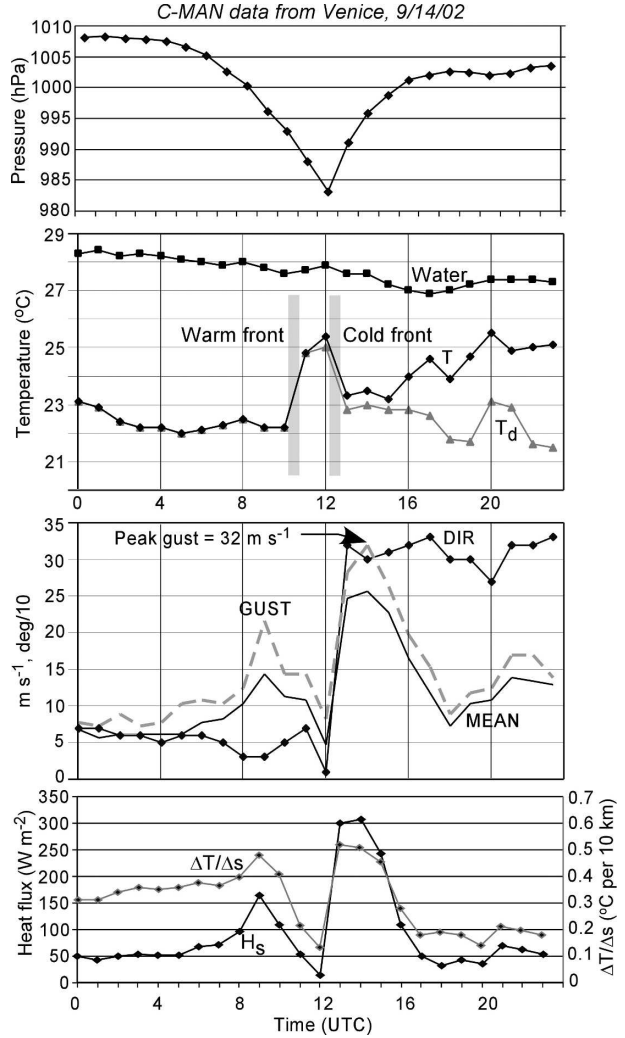


FIG. 8. Time series of recorded and estimated quantities of the Venice (VENF1) C-MAN station, located adjacent to the MIPS. The bottom panel includes surface heat flux (H_s), estimated from Eq. (1), and temperature gradient ($\Delta T/\Delta s$) off the west coast based on the value of heat flux and wind speed.

where α is specific volume, and $dQ/dt = H_s$ from Eq. (1). The rate of temperature change, dT/dt is determined from Eqs. (1) and (2), with three additional assumptions: (i) the heat (surface flux) is distributed uniformly over the lowest 200 m as the internal ABL develops, (ii) evaporation of stratiform precipitation is negligible, and (iii) the process occurs isobarically (i.e., $dp/dt = 0$). The temperature change rate can be converted to a horizontal temperature gradient along the flow ($\partial T/\partial s$) assuming that the local change is small. This gradient, also plotted in Fig. 8 ($\Delta T/\Delta s$, bottom panel), parallels the behavior of H_s , but is not strictly similar to it.

As the convergent ABL flow within Gabrielle ap-

proached the offshore temperature gradient, the stage was set for frontogenesis and development of a warm front offshore. Essential processes are depicted in Fig. 9. If asymmetries that are produced by translation and vertical shear (Shapiro 1983; Bender 1997; Frank and Ritchie 1999) existed in the translating circulation, then enhanced convergence in the storm's forward flank would have promoted frontogenesis within the shaded region of Fig. 9.

The frontogenesis function of the form (Bluestein 1993),

$$F = \left(\frac{\partial v}{\partial s}\right)\left(\frac{\partial \theta}{\partial s}\right) + \left(\frac{\partial w}{\partial s}\right)\left(\frac{\partial \theta}{\partial z}\right) - \frac{1}{c_p} \left(\frac{p_0}{p}\right)^\kappa \left(\frac{\partial}{\partial s}\right)\left(\frac{dQ}{dt}\right), \quad (3)$$

provides insight on how these fronts may have formed. In Eq. (3), v and s are the wind component and horizontal distance normal to the potential temperature (θ) gradient, w is vertical motion, and z is the vertical coordinate. Analyses of MIPS and SMART-R data presented below suggest that the mesoscale outflow of the cool air over the Florida Peninsula acted much like a density current confined to the ABL. As Gabrielle approached this zone, we hypothesize that ABL convergence in the front flank of the storm enhanced F via the first term of Eq. (3). We estimate this term to about $0.2 \text{ K km}^{-1} \text{ h}^{-1}$, using values of $\partial\theta/\partial s$ ($\Delta T/\Delta s$) from Fig. 8. The term $\partial w/\partial s$ is estimated to be about $1 \text{ m s}^{-1} \text{ km}^{-1}$, which is consistent with ABL convergence magnitudes (on the order of 10^{-3} s^{-1}) simulated by Shapiro (1983) and Frank and Ritchie (1999).

This warm front appears in the surface analysis at 0900 UTC (Fig. 6b). Prior to this at 0600 UTC, a broad temperature contrast is evident over the region from Lake Okeechobee, where the surface temperature was near 23°C , southward to the Florida Keys where the temperature was 28°C . Unfortunately, the southwest part of Florida was not adequately instrumented with surface stations. After landfall, a cold front developed within the northwestern flank of Gabrielle as cool air wrapped around the western flank. By 1500 UTC, this cold front had surged eastward to a relative location curving east, southeast, and south of the wind center (Fig. 6d).

2) SURFACE TIME SERIES

Time series from surface stations provide more details on spatial variability of the frontal properties. Figure 10 presents meteorological variables from Sarasota (30 km north-northwest of MIPS) and Punta Gorda (PGD; 50 km southeast of MIPS), respectively. Fronts were absent at SRQ, and the wind backed systemati-

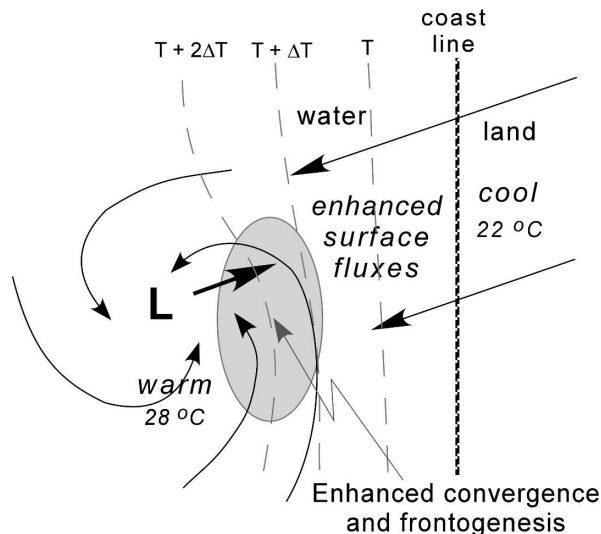


FIG. 9. Schematic showing the basic elements within the boundary layer that promote frontogenesis. These include the source of cool air from land, surface heat fluxes over the water producing a horizontal temperature gradient, and the convergent forward flank of Gabrielle, perhaps enhanced in this case by the east-northeasterly airflow that existed on a scale larger than that of Gabrielle's core cyclonic circulation. Dashed lines are isotherms near the surface.

cally from northeast to northwest as the wind center moved south and east of SRQ. However, the cool temperatures at SRQ served as a prerequisite for frontogenesis. At PGD, a vague warm frontal signature is apparent in the temperature and dewpoint. The wind shift at PGD near 0900 UTC was associated with intense convection; the warm front passed over about 30 min later. The cold frontal passage, marked by a modest temperature and dewpoint temperature decreases of 2° and 1°C , respectively, was also detected at PGD near 1330 UTC.

Frontal passage signatures were more significant near the wind center, consistent with the conceptual model in Fig. 9. The hourly C-MAN observations in Fig. 8 show temperature changes of $+3^\circ$ and -2°C associated with the warm and cold fronts. Very high temporal resolution (1 Hz) measurements of both fronts were acquired at the MIPS site (Fig. 11). The warm front was marked by increases in T and T_d of 2.5° and 2°C , respectively, over a 20-min period. Assuming a movement speed of 5 m s^{-1} , based on the surface analyses in Figs. 6b–c, the frontal zone width is estimated at 6 km. (The cold frontal passage was not completely sampled at the MIPS site due to a datalogger failure.) The warm and cold fronts were also sampled 50 km to the northeast at Ona (Fig. 7) near 1200 and 1400 UTC, respectively. A more substantial temperature drop of

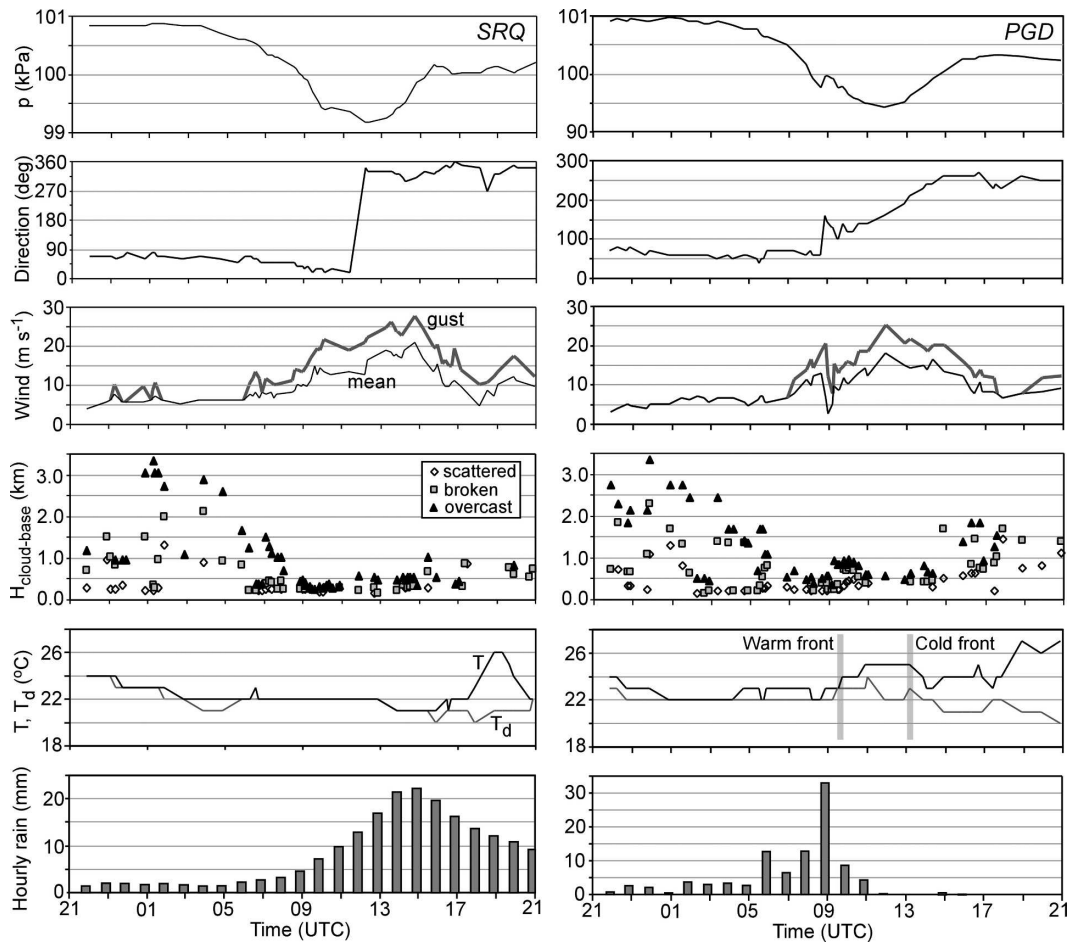


FIG. 10. Time series of surface parameters from ASOS sites located at Sarasota (SRQ) and Punta Gorda (PGD). Locations are shown in Fig. 6b. Rain rate is plotted as an hourly value. All other parameters are plotted for standard hourly plus supplemental observation times.

3°C was recorded after the cold front passage, but T_d decreased much sooner (near 1245 UTC) as drier air was apparently entrained into the ABL.

In summary, warm and cold fronts were generated by production of cool air over land from evaporation within stratiform precipitation. As shown by the surface data in Figs. 6, 7, 8, 10, and 11, the fronts were most prominent near and in advance of the wind center where convergence is typically most substantial. The frontal zone widths of about 5 km observed here are not as narrow as gust fronts and boundaries that often exhibit width scales less than 1–2 km (e.g., Karan and Knupp 2006).

c. Other ABL phenomena related to cool surface air

Two other ABL phenomena closely related to cold air at the surface are briefly addressed here because

they have been observed in other landfalling hurricanes, but their relative importance is unknown. The first is the ubiquity of low stratus fractus and/or stratocumulus clouds, which result from ABL turbulence in combination with the near saturation of surface air (i.e., $T - T_d < 3^\circ\text{C}$). As shown in Fig. 10, cloud-base heights decreased to values near 200 m AGL, a level well below the ABL top. Knupp et al. (2000) also examined low cloud bases during the landfall of Hurricane Georges and speculated that saturation may complicate ABL thermodynamics.

Second, gravity waves appear to be common in landfalling TCs when cool surface temperatures promote stable conditions over land. The pressure trace in Fig. 11 reveals a gravity wave train consisting of at least eight consecutive small-amplitude (0.5–1.0 mb) waves between 0840 and 0945 UTC, about 35–100 min prior to the passage of the warm front. These waves exhibit a

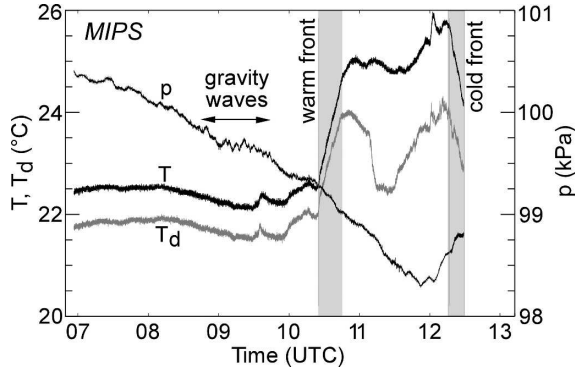


FIG. 11. MIPS surface parameters for the 0700–1300 UTC period. Frontal boundaries are depicted by the gray shading. Data frequency is 1 Hz.

mean period of about 8 min, which is close to the typical Brunt–Väisälä period, $P = 2\pi/N$, where N is the Brunt–Väisälä frequency

$$N = \left(\frac{g}{\theta} \frac{\partial \theta}{\partial z} \right)^{1/2}.$$

The observed period corresponds to a local $\partial\theta/\partial z$ value of about 5 K km^{-1} , which is approximately the gradient shown in the sounding (Fig. 3) between 1000 and 900 hPa. Such gravity waves corroborate the stable conditions near the top of the ABL (and locally enhanced at the base of the warm front), in the midst of relatively strong ABL wind speeds that existed around this time.

5. Boundary layer structure and variability

Three-dimensional airflow properties of the ABL within the coastal zone were determined from MIPS and SMART-R observations. These analyses address the following questions. What is the temporal variability in ABL winds during landfall? What are the differences in ABL structure over the land-to-water transition zones from stable (offshore) to unstable (onshore) conditions? Over what distance does the ABL transformation take place?

Winds were computed within a vertical plane using radial velocity measurements from the SMART-R. Edited radial velocity was transformed to a Cartesian domain, centered on the MIPS/SMART-R, that was $\pm 15 \text{ km}$ in the x and y directions, and $0\text{--}2 \text{ km}$ in the vertical direction. Grid spacing was 0.5 km in x and y , and 0.1 km in the vertical.

Analyses of horizontal flow isotachs are presented within a vertical plane whose orientation was determined by the 915-MHz profiler mean wind direction

within the lowest 600 m. The horizontal wind V_h was determined from SMART-R radial velocity (V_r) using

$$V_h = \frac{V_r - W \sin \alpha}{\cos \alpha},$$

where α is the radar elevation angle, $W = w + V_T$ is the vertical particle velocity measured by the 915-MHz profiler at vertical incidence around the time of the scanning Doppler radar observations, w is vertical air motion, and V_T is the hydrometeor terminal fall speed. We assume that W is uniform over a horizontal domain within 15 km of the MIPS, which is deemed a good assumption within stratiform precipitation.

The evolution of the ABL flow is summarized in Fig. 12, a plot of contiguous 10-min wind speed and direction at 295 m AGL, roughly the half-depth of the ABL. The offshore flow (0500–1000 UTC) preceded the arrival of the warm front at 1030 UTC, and occurred within the leading stratiform precipitation and generally cool, neutral-to-stable conditions. During this regime, the wind speed at 295 m increased from 16 m s^{-1} at 0500 UTC to $19\text{--}27 \text{ m s}^{-1}$ in flow with more variable speed between 0900 and 1130 UTC. The onshore flow prevailed within the western side of Gabrielle after the wind center passed over the MIPS. This (unstable) regime occurred after the cold frontal passage within northwesterly flow having a long fetch off the western Florida coastal waters. Wind speeds were persistently strong at $30\text{--}33 \text{ m s}^{-1}$ between 1300–1500 UTC and declined monotonically thereafter.

a. Offshore flow boundary layer within the leading stratiform region

ABL properties are analyzed at 0551 UTC, near the center of the leading stratiform band (see Figs. 2 and 4 for location relative to the MIPS). Surface flow was east-northeasterly, veering to southeasterly above 1 km AGL (Fig. 5), and cool, nearly saturated surface conditions prevailed. Over the region within 50 km of the

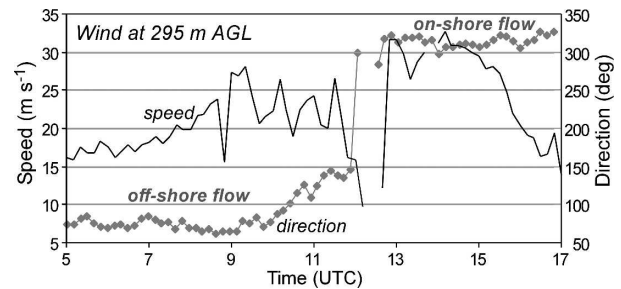


FIG. 12. The 915-MHz profiler wind speed and direction within the boundary layer at 295 m AGL. This time series is derived from contiguous 10-min averages.

MIPS, the stratiform rain rate (15-min average) was locally heavy, up to 23 mm h^{-1} at Ona (Fig. 7).

1) TEMPORAL VARIABILITY AT THE COASTLINE

The nearly steady wind at 295 m AGL (Fig. 12) around 0551 UTC suggests a stable ABL with nearly stationary flow conditions. This was not strictly the case. Wind profiles from the 915-MHz profiler ± 20 min of 0550 UTC are presented in Fig. 13. The wind direction profiles exhibit similar shape, each veering with height about 60° – 70° over a 1.5-km vertical depth. Over this 40-min period, the direction backed about 15° throughout the lowest 2 km. A different impression of flow stationarity is revealed by the more variable wind speed profiles. While the initial two profiles at 0530 and 0540 UTC are similar (uniform speed up to 0.7 km, with moderate positive shear above), a rapid transition from this shape is noted for 0550 and 0600 UTC. A modest jet structure is analyzed near 0.5 km and significantly lower wind speed values are displayed above 0.7 km. By 0610 UTC, the low-level jet profile had disappeared. Because the wind speed profiles changed both within and above the ABL (estimated to be 0.5 km deep), such differences are attributed to mesoscale variations within this stratiform rainband. This has potential implications on the interpretation of the spatial distribution of wind profiles, discussed next.

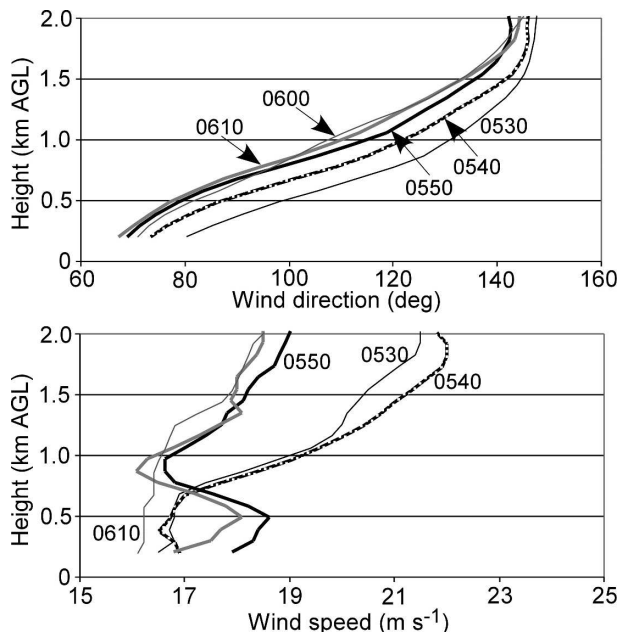


FIG. 13. Vertical profiles of (top) wind direction and (bottom) wind speed, based on 10-min averages from the 915-MHz profiler, for the stable offshore flow regime within the leading stratiform band from 0530 to 0610 UTC.

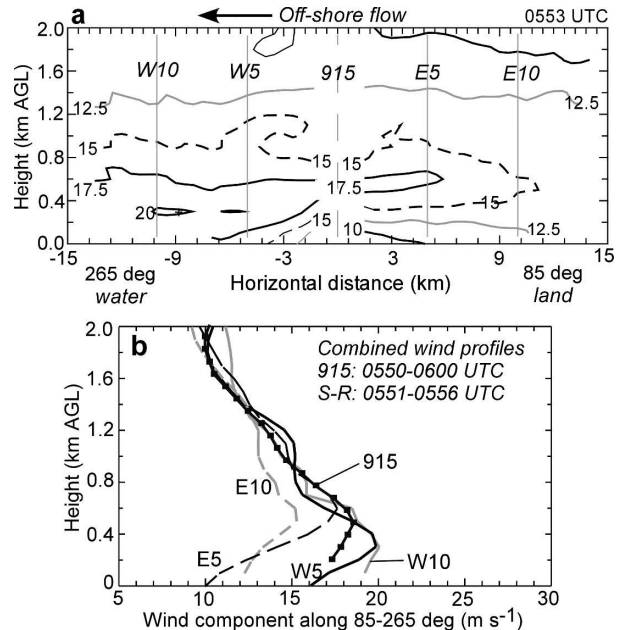


FIG. 14. (a) Isotach analysis of the horizontal velocity component within the vertical plane that passes over the SMART-R and MIPS along the direction 265° – 85° , roughly parallel to the wind direction at 400 m AGL. Contours are labeled in m s^{-1} . (b) W10, W5, E5, and E10 represent locations of vertical profiles of this wind component. Here, 915 represents the location of the wind component within this plane derived from the MIPS 915-MHz profiler. (b) Vertical profiles of the wind component analyzed in (a). The 915-MHz wind profile represents a 10-min average. All profiles exhibit a jet structure. The jet height progressively increases from water (W, west) to land (E, east).

2) SPATIAL VARIABILITY ACROSS THE COASTAL ZONE

The combined Doppler radar and 915-MHz wind profiler analysis, valid for 0550–0600 UTC, is shown in Fig. 14. Figure 14a presents isotachs of the horizontal airflow component within the vertical plane along the mean wind direction over the lowest 500 m. Profiles at the five locations identified in Fig. 14a are plotted in Fig. 14b. Highlights of this analysis include the following.

- (i) In view of the temporal variability at the MIPS location noted in the previous section, the spatial variability at this time appears to be dictated primarily by changes in surface characteristics. With the exception of profile E10, wind profiles are nearly identical above the ABL (0.6 km).
- (ii) The flow is jetlike and appears to behave like a density current, consistent with the inference that this is an outflow maintained partly by mesoscale downdrafts over the peninsula.
- (iii) Over land (right half of Fig. 14a), considerably

more vertical shear is analyzed at levels below the wind maximum (jet) located near 600 m AGL. Small shear values are analyzed over the water beyond 10 km from the coastline.

- (iv) Over water, the ABL flow accelerated to the west and the jet descended to a lower level of about 300 m. The jet was less pronounced 10 km offshore (W10), presumably from increased turbulent mixing induced by surface heat fluxes (about 60 W m^{-2} , Fig. 8, section 4b), which promoted the development of an unstable internal boundary layer; and stronger flow over the lowest 200 m, resulting from decreased surface roughness over the water.
- (v) The previous two items suggest that the height of the jet scales with the ABL top. If this is the case, the ABL depth over water is about half that over land. This elicits the question: Are roughness effects over land surfaces (for a weakly stable ABL) more prominent than the effects of enhanced surface heat flux over the water on the depth of the ABL?
- (vi) The acceleration in airflow over the lowest 400 m is most substantial within about 5 km of the coastline; that is, the ABL appears to adjust to new surface properties from land to water (decreased friction, increased surface sensible and latent heat fluxes) over a total pathlength of about 10 km centered on the coastline.
- (vii) The ABL transition and flow acceleration occurs on land before the air moves over the water. This is clearly shown in the 915 wind profile (Fig. 14b), which displays a jet maximum value, and jet height, roughly intermediate between the measured values 5 km over land (E5) and 5 km over water (W5).

b. Onshore flow boundary layer

Measurements of the ABL during relatively strong onshore flow conditions at 1355 UTC were acquired during a break in precipitation just north of a shallow rainband (see Fig. 2e). Low-level flow was northwesterly, backing to westerly above 1 km AGL.

1) TEMPORAL VARIABILITY AT THE COASTLINE

The low-level wind was quite variable around the time of observations. Figure 15 presents wind profiles for a 1-h period centered on the 1355 UTC analysis time. During this period the wind profile evolved systematically from one in which the wind maximum occurred at the lowest level of 200 m at 1330 UTC to one that exhibited a jet profile with a maximum of 32–33 m s^{-1} within the 500–1000 m AGL layer. The level of

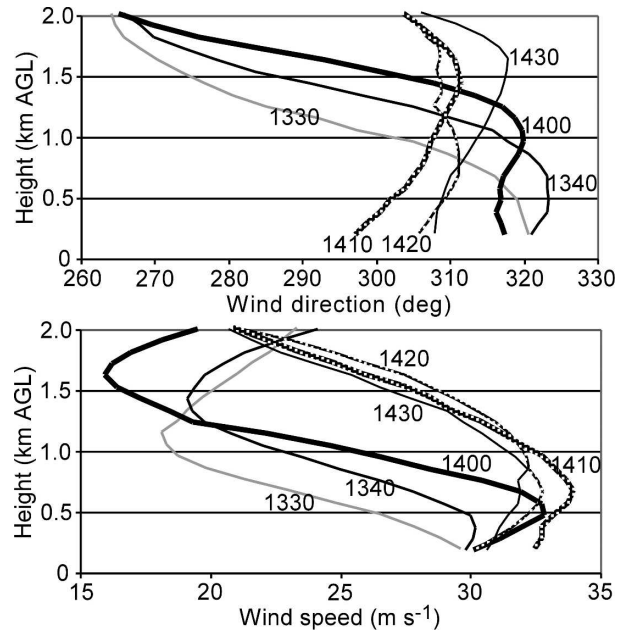


FIG. 15. As in Fig. 13, except for the unstable onshore flow regime along the west side of Gabrielle from 1330 to 1430 UTC.

the wind maximum was initially within the ABL, but with time the jet ascended to near the top of the ABL. This observation shows a trend similar to that predicted by the linear theory advanced by Kepert (2001), in which the jet height increases monotonically from values of 200–300 m at a small radius (about 10 km), to values of 500–1000 m near 100-km radius. However, in the case of Gabrielle, the transformation occurred over a horizontal length scale that was about one-third the 90-km distance in Kepert's model results.

2) SPATIAL VARIABILITY ACROSS THE COASTAL ZONE

The mean wind direction in the lowest 600 m was from about 320° over the water, with some cyclonic turning toward 125° over land southeast of the radar. Figure 16a displays the horizontal wind component within these two separate vertical planes, oriented along azimuths of 320° and 125° in order to follow cyclonic curvature of the airflow. Figure 16b shows profiles at the locations indicated in Fig. 16a. The key points include the following.

- (i) Over the width of this domain, a general flow deceleration was most significant at low levels, and was even apparent within the 1–2-km layer, that is, above the ABL.
- (ii) The deceleration in low-level onshore flow began over water, about 5 km upwind of the coastline.

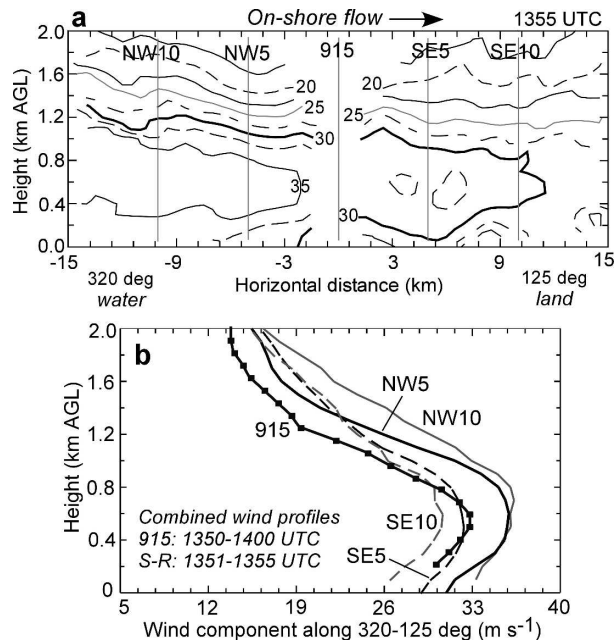


FIG. 16. As in Fig. 14, except for 1355 UTC. (a) The vertical plane is oriented along 320° on the water side, and along 125° on the land side, to follow the mean wind direction as it changes cyclonically from water to land.

This produced a greater vertical shear over land, consistent with common knowledge.

- (iii) Within the lowest 200 m over land, oscillations in wind speed suggest the presence of large eddies in the ABL. Although the flow was more uniform over the water, we note that streaks in radial velocity, approximately aligned with the flow direction, were prominent in V_r fields over water. Such longitudinal streaks are commonly observed in landfalling TCs (Wurman and Winslow 1998), and have also been simulated with a 3D numerical model (Yau et al. 2004).
- (iv) The ABL height was not well defined by the isotachs. The jet axis appears to have descended from 800 m over the water (-12 km) to 500–600 m over land ($+12$ km).
- (v) Interestingly, the vertical shear above the jet over water was about 50% greater than that over land.

One unexpected finding is the descent of the jet from water to land. This behavior is counterintuitive to the perceived deepening of the ABL from increased friction and momentum transport over land.

6. Discussion

a. Fronts in tropical cyclones?

Although fronts have not been documented in previous studies of low-latitude landfalling tropical cy-

clones, we believe they may be relatively common. Powell (1987) shows large gradients in θ_e within the right flank of Hurricane Alicia as landfall occurred near Galveston, but surface spatial resolution was insufficient to resolve a front. We have also sampled possible fronts (albeit less prominent) during other MIPS deployments in the right quadrant of landfalling tropical cyclones, including Hurricane Earl (1998), TS Helena (1999), and TS Isidore (2002). Hurricane Earl was a sheared asymmetric system much like Gabrielle, and leading stratiform precipitation reduced temperatures to near 22° – 23°C around Tallahassee. A suspected warm front increased the temperature from 22° to 26°C while the wind center was still located southwest of the MIPS location (Roberts 2005).

Fronts are apparently more common during Atlantic coast landfalls at higher latitudes, and during extratropical transition. The generation of fronts within Tropical Storm Agnes (1972) was documented by Bosart and Dean (1991). They determined that a cold front formed in situ over eastern Virginia, with the assistance of advection of cooler drier air from the west, almost 3 days after landfall near Tallahassee, Florida. In another noteworthy case, Hurricane Floyd (1999) merged with a preexisting deep coastal front shortly after landfall over North Carolina. This interaction produced widespread heavy rain along the east coast (Colle 2003).

In contrast to the Agnes and Floyd cases, the fronts produced by TS Gabrielle were produced (primarily) by local mesoscale processes, that is, production of cool air within mesoscale downdrafts within the large stratiform rain shield that preceded landfall, and subsequent fluxes in the region of offshore flow (over warm water), which provided the horizontal temperature gradient. We therefore hypothesize that fronts are more likely when vertical wind shear promotes development of stratiform precipitation over land in advance of landfalling TCs. This hypothesis is supported by the behavior of Hurricane Earl in 1998 (Roberts 2005) and by the recent landfall of Hurricane Ivan in 2004.

b. ABL transition

The observed acceleration upstream from the coastline is a feature common to both offshore and onshore ABL flows. For the offshore flow, this acceleration was analyzed over land, while for the onshore flow, the deceleration began several kilometers over the water. In each case, it appears that the ABL flow accelerated before air crossed the coastline and adjusted to new surface conditions. Such acceleration implies the presence of an induced mesoscale pressure gradient along the coastal zone.

The observations presented here provide more de-

tails on the complexities of ABL flows within the coastal region. Using surface data, Powell et al. (1991) suggested that onshore surface flow adjusts to the rough surface over a fetch of about 1 km. For more stable offshore flows, this fetch distance was estimated to be 3–4 times greater. In earlier work, Sethuraman (1979) used a linear array of surface wind measurements to determine that onshore coastal winds were reduced by a factor of 2 within 10 km of the coastline. Our measurements reveal a clear transition of airflow within and above the ABL within the coastal region, but apparent mesoscale variations in airflow complicate interpretation of microscale properties. For example, nonstationary flow conditions measured by the MIPS were apparently related to gravity waves and boundary layer eddies such as rolls and streaks of the type documented by Wurman and Winslow (1998).

7. Summary and conclusions

The unique measurements acquired during the landfall of Gabrielle have revealed several properties of the evolving ABL, some of which have not previously been well documented with observations. These are summarized below.

a. Cool air

A large area of unusually cool air ($T \leq 22^\circ\text{C}$) was produced by prolonged evaporation of stratiform precipitation downshear of Gabrielle. At landfall, the area within the 23°C isotherm was about 50 000 km². This cool air was a prerequisite for three other phenomena. (i) It set the stage for frontogenesis within the ABL near landfall. (ii) The cool, nearly saturated surface air produced a weakly stable ABL during the offshore flow regime. (iii) The large area of cool (low θ_e) air appeared to play a role in the rapid weakening of Gabrielle just before landfall by reducing ABL θ_e values to <345 K. Accurate forecasting of ABL cooling would appear to have applications in TC intensity change.

b. Boundaries

Shallow warm and cold fronts within the ABL accompanied Gabrielle at landfall, and resembled the relative orientation of much deeper fronts in mature baroclinic midlatitude cyclones. Frontogenesis was promoted by a horizontal temperature gradient, produced by surface sensible heat fluxes from cool air flowing over warm water. When the convergent core of Gabrielle encountered this gradient, fronts formed within a period of several hours.

c. Airflow variation within the coastal zone

Because the wind center of Gabrielle passed over the MIPS, both offshore and onshore flow regimes were sampled. During both regimes, temporal variability of the wind profile at the MIPS site along the coastline was significant. This temporal variability was related to the presence of gravity waves and large ABL eddies.

The offshore regime was rendered near stable by evaporational cooling of air within mesoscale downdrafts over the Florida Peninsula. During the offshore regime, the flow frequently peaked at low levels, forming a jet profile. For the time periods analyzed, the jet height descended from about 600 m over land, to about 300 m over water. Wind shear below the jet was moderate over land, but negligible over water. Most of this transformation occurred within 5 km of the coastline. Numerical simulations would be required to assess the relative roles of reduced surface roughness (land to water) and increased surface heat flux over water, on the development of a shallow unstable ABL over the water.

The onshore regime was marked by a more turbulent (unstable) ABL, and a flow in which the maximum wind speed ascended with time from near the 200 m AGL initially (at small radius) to 0.5–1.0 km within a 1-h period (2–3 h after landfall). Again, much of the flow transition from water to land occurred within 5 km of the coastline. For both the offshore and onshore regimes, flow acceleration, and deceleration occurred several kilometers on the upstream side of the coastline.

d. Future research

Future research should include detailed investigations of the production of cold air within mesoscale downdrafts of the stratiform precipitation region. The thermodynamics are closely related to the kinematic and microphysical properties of stratiform regions, which have not yet been described for TCs. The production of cold air has potentially important applications for forecasting intensity change around the time of landfall. Thermodynamic data from dropsondes, combined with wind profiler and single/multiple Doppler analyses from mobile ground-based and airborne radars, are required to better understand the complicated landfall processes, and to improve parameterization in numerical models.

With regard to ABL transition during landfall, similar comprehensive measurements of surface and ABL properties are needed to better understand variability in the dependence of ABL structure on mesoscale processes, static stability (from dropsondes), and wind

speed. ABL transition is likely a three-dimensional process and therefore should be examined in more detail with high resolution multiple Doppler radar. The relative importance of microphysical processes on ABL properties, including rainfall evaporation and cloud condensation, should be assessed as well.

Acknowledgments. The authors extend a sincere thanks to two reviewers who provided thorough reviews that significantly improved the quality of this paper. Mr. Simon Paech provided assistance with preparation of GOES and surface analyses using the McIDAS and GEMPAK software, provided by the Unidata program. Ms. Courtney Radley assisted in editing of SMART-R data. NCAR is gratefully acknowledged for providing the SOLO-II, REORDER, and CEDRIC software packages for Doppler radar processing. This research was supported by the National Aeronautics and Space Administration under Grant NCC8-200 and by the National Science Foundation under Grant ATM-0002252. The program manager for the NASA CAMEX-4 project was Dr. Ramesh Kakar.

REFERENCES

- Barnes, G. M., and M. D. Powell, 1995: Evolution of the inflow boundary layer of Hurricane Gilbert (1988). *Mon. Wea. Rev.*, **123**, 2348–2368.
- , E. J. Zipser, D. Jorgensen, and F. Marks, 1983: Mesoscale and convective structure of a hurricane rainband. *J. Atmos. Sci.*, **40**, 2125–2137.
- Bender, M. A., 1997: The effect of relative flow on the asymmetric structure in the interior of hurricanes. *J. Atmos. Sci.*, **54**, 703–724.
- Blackwell, K. G., 2000: The evolution of Hurricane Danny (1997) at landfall: Doppler-observed eyewall replacement, vortex contraction/intensification, and low-level wind maxima. *Mon. Wea. Rev.*, **128**, 4002–4016.
- Bluestein, H. B., 1993: *Synoptic–Dynamic Meteorology in Midlatitudes*. Vol. II, *Observations and Theory of Weather Systems*, Oxford University Press, 594 pp.
- Bosart, L. F., and D. B. Dean, 1991: The Agnes rainstorm of June 1972: Surface feature evolution culminating in inland storm redevelopment. *Wea. Forecasting*, **6**, 515–537.
- Braun, S. A., and W.-K. Tao, 2000: Sensitivity of high-resolution simulations of Hurricane Bob (1991) to planetary boundary layer parameterizations. *Mon. Wea. Rev.*, **128**, 3941–3961.
- Bryan, G. H., and M. J. Fritsch, 2000: Moist absolute instability: The sixth static stability state. *Bull. Amer. Meteor. Soc.*, **81**, 1207–1230.
- Chen, Y., and M. K. Yau, 2003: Asymmetric structures in a simulated landfalling hurricane. *J. Atmos. Sci.*, **60**, 2294–2312.
- Cione, J. J., P. G. Black, and S. H. Houston, 2000: Surface observations in the hurricane environment. *Mon. Wea. Rev.*, **128**, 1550–1561.
- Colle, B. A., 2003: Numerical simulations of the extratropical transition of Floyd (1999): Structural evolution and responsible mechanisms for the heavy rainfall over the northeast United States. *Mon. Wea. Rev.*, **131**, 2905–2926.
- Dodge, P., S. Houston, W. C. Lee, J. Gamache, and F. D. Marks Jr., 1999: Windfields in Hurricane Danny (1997) at landfall from combined WSR-88D and airborne Doppler radar data. Preprints, *23d Conf. on Hurricanes and Tropical Meteorology*, Dallas, TX, Amer. Meteor. Soc., 61–62.
- Dunion, J. P., C. W. Landsea, S. H. Houston, and M. D. Powell, 2003: A reanalysis of the surface winds for Hurricane Donna of 1960. *Mon. Wea. Rev.*, **131**, 1992–2011.
- Frank, W. M., and E. A. Ritchie, 1999: Effects of environmental flow upon tropical cyclone structure. *Mon. Wea. Rev.*, **127**, 2044–2061.
- Franklin, J. L., M. L. Black, and K. Valde, 2003: GPS dropwindsonde wind profiles in hurricanes and their operational implications. *Wea. Forecasting*, **18**, 32–44.
- Geerts, B., G. M. Heymsfield, L. Tian, J. B. Halverson, A. Guillory, and M. I. Mejia, 2000: Hurricane Georges's landfall in the Dominican Republic: Detailed airborne Doppler radar imagery. *Bull. Amer. Meteor. Soc.*, **81**, 999–1018.
- Harasti, P. R., C. J. McAdie, P. P. Dodge, W.-C. Lee, J. Tuttle, S. T. Murillo, and F. D. Marks, 2004: Real-time implementation of single-Doppler radar analysis methods for tropical cyclones: Algorithm improvements and use with WSR-88D display data. *Wea. Forecasting*, **19**, 219–239.
- Jones, R. W., 1987: A simulation of hurricane landfall with a numerical model featuring latent heating by the resolvable scales. *Mon. Wea. Rev.*, **115**, 2279–2297.
- Karan, H., and K. R. Knupp, 2006: Mobile Integrated Profiler System (MIPS) observations of low-level convergent boundaries during IHOP. *Mon. Wea. Rev.*, **134**, 92–112.
- Kepert, J., 2001: The dynamics of boundary layer jets within the tropical cyclone core. Part I: Linear theory. *J. Atmos. Sci.*, **58**, 2469–2484.
- , and Y. Wang, 2001: The dynamics of boundary layer jets within the tropical cyclone core. Part II: Nonlinear enhancement. *J. Atmos. Sci.*, **58**, 2485–2501.
- Knupp, K. R., J. Walters, and E. W. McCaul Jr., 2000: Doppler profiler observations of Hurricanes Georges at landfall. *Geophys. Res. Lett.*, **27**, 3361–3364.
- Li, J., N. E. Davidson, G. D. Hess, and G. Mills, 1997: A high-resolution prediction study of two typhoons at landfall. *Mon. Wea. Rev.*, **125**, 2856–2878.
- Marks, F. D., Jr., 2003: State of the science: Radar view of tropical cyclones. *Radar and Atmospheric Science, Meteor. Monogr.*, No. 30, Amer. Meteor. Soc., 33–73.
- , and L. K. Shay, 1998: Landfalling tropical cyclones: Forecast problems and associated research opportunities. *Bull. Amer. Meteor. Soc.*, **79**, 305–323.
- Molinari, J., P. Dodge, D. Vollaro, K. L. Corbosiero, and F. Marks, 2006: Mesoscale aspects of the downshear reformation of a tropical cyclone. *J. Atmos. Sci.*, **63**, 341–354.
- Moss, M. S., and F. J. Merceret, 1976: A note on several low-level features of Hurricane Eloise (1975). *Mon. Wea. Rev.*, **104**, 967–971.
- Powell, M. D., 1982: The transition of the Hurricane Frederic boundary-layer wind field from the open Gulf of Mexico to landfall. *Mon. Wea. Rev.*, **110**, 1912–1932.
- , 1987: Changes in the low-level kinematic and thermodynamic structure of Hurricane Alicia (1983) at landfall. *Mon. Wea. Rev.*, **115**, 75–99.
- , 1990a: Boundary layer structure and dynamics in outer hurricane rainbands. Part I: Mesoscale rainfall and kinematic structure. *Mon. Wea. Rev.*, **118**, 891–917.

- , 1990b: Boundary layer structure and dynamics in outer hurricane rainbands. Part II: Downdraft modification and mixed layer recovery. *Mon. Wea. Rev.*, **118**, 918–938.
- , and P. G. Black, 1990: The relationship of hurricane reconnaissance flight-level measurements to winds measured by NOAA's oceanic platforms. *J. Wind Eng. Ind. Aerodyn.*, **36**, 381–392.
- , and S. H. Houston, 1998: Surface wind fields of 1995 Hurricanes Erin, Opal, Luis, Marilyn, and Roxanne at landfall. *Mon. Wea. Rev.*, **126**, 1259–1273.
- , P. D. Dodge, and M. L. Black, 1991: The landfall of Hurricane Hugo in the Carolinas: Surface wind distribution. *Wea. Forecasting*, **6**, 379–399.
- , S. H. Houston, and T. A. Reinhold, 1996: Hurricane Andrew's landfall in south Florida. Part I: Standardizing measurements for documentation of surface wind fields. *Wea. Forecasting*, **11**, 304–328.
- Roberts, B. C., 2005: Doppler profiler observations of a gravity wave associated with Hurricane Earl at landfall. M.S. thesis, Dept. of Atmospheric Science, University of Alabama in Huntsville, 75 pp.
- Sethuraman, S., 1979: Atmospheric turbulence and storm surge due to Hurricane Belle (1976). *Mon. Wea. Rev.*, **107**, 314–321.
- Shapiro, L. J., 1983: The asymmetric boundary layer flow under a translating hurricane. *J. Atmos. Sci.*, **40**, 1984–1998.
- Tuleya, R. E., 1994: Tropical storm development and decay: Sensitivity to surface boundary conditions. *Mon. Wea. Rev.*, **122**, 291–304.
- Williams, C. R., W. L. Ecklund, and K. S. Gage, 1995: Classification of precipitating clouds in the Tropics using 915-MHz wind profilers. *J. Atmos. Oceanic Technol.*, **12**, 996–1012.
- Wu, C.-C., 2001: Numerical simulation of Typhoon Gladys (1994) and its interaction with Taiwan terrain using the GFDL hurricane model. *Mon. Wea. Rev.*, **129**, 1533–1549.
- Wurman, J., and J. Winslow, 1998: Intense sub-kilometer-scale boundary layer rolls observed in Hurricane Fran. *Science*, **280**, 555–557.
- Yau, M. K., Y. Liu, D.-L. Zhang, and Y. Chen, 2004: A multiscale numerical study of Hurricane Andrew (1992). Part VI: Small-scale inner-core structures and wind streaks. *Mon. Wea. Rev.*, **132**, 1410–1433.
- Zhang, D.-L., Y. Liu, and M. K. Yau, 1999: Surface winds at landfall of Hurricane Andrew (1992)—A reply. *Mon. Wea. Rev.*, **127**, 1711–1721.